Evaluating the Potential of annual Sentinel-1 Composites for Bark Beetle Infestation Detection

Sebastian Spreitzer[1], Georg Wohlfahrt[2], Martin Rutzinger[1]

[1] University of Innsbruck, Department of Geography, Innrain 52f, Innsbruck, Austria
- sebastian.spreitzer@uibk.ac.at, martin.rutzinger@uibk.ac.at
[2] University of Innsbruck, Department of Ecology, Sternwartestraße 15, Innsbruck, Austria
- georg.wohlfahrt@uibk.ac.at

Keywords: Bark Beetle, SAR, Sentinel-2, Sentinel-1, Random Forest.

Abstract

The exponential spread of the bark beetle *(Ips typographus L.)* outbreaks across Europe in recent years has led to heightened interest in remote sensing-based detection. This increase is closely linked with ongoing climate change, which has led to rising temperatures, prolonged dry periods, and increasing frequency and intensity of both biotic and abiotic disturbances. These conditions created a favourable environment for bark beetle proliferation, resulting in larger and more widespread infestations. Effective detection and management of these outbreaks is crucial for forest officals, necessitating the implementation of monitoring systems that complement traditional ground-based efforts. At present, remote sensing approaches for bark beetle detection mainly rely on optical data to identify changes in spectral reflectance of vegetation. In this study, we utilised annual Sentinel-1 synthetic aperture radar (SAR) composites from 2021 to 2023 for infestation detection. A Random Forest classification model was applied to distinguish between healthy and infested forest areas. Additionally, vegetation indices were incorporated to evaluate and compare the results. A reference dataset was used to validate model performance. Our results show that the Sentinel-1 based approach achieved lower accuracies (max. overall accuracy: 0.78), compared to Sentinel-2 (max. overall accuracy: 0.87). Despite this, the Sentinel-1 data proved valuable as a tool for bark beetle infestations detection, especially in scenarios where optical data may be unavailable or limited. These results underscore the importance of integrating SAR data into remote sensing workflows to improve the detection of bark beetle outbreaks.

1. Introduction

Natural disturbances, both abiotic (e.g., windthrow, fires) and biotic (e.g., insects, pathogens), play a crucial role in the development, functioning and dynamics of forest ecosystems (Turner, 2010). Disturbances are integral to maintaining ecosystem processes, yet they also represent significant challenges, especially under changing environmental conditions. The exponential spread of bark beetle outbreaks in Europe in recent years led to an increased interest in the remote sensing-based detection of outbreaks. Forest ecosystems react highly sensitive to environmental changes, making them particularly vulnerable to climate change, due to rising temperatures, prolonged dry periods, and an increase in frequency and intensity of biotic and abiotic disturbance events (Seidl et al., 2011, Seidl et al., 2017).

Due to their long live-cycles, trees are inherently slow to adapt to rapid environmental shifts. Stressors such as heat or drought have a negative impact on tree vitality and functioning, leaving them more susceptible to forests pests (Huang et al., 2020). Furthermore, insects are among the primary beneficiaries of climate change, as their development cycle is strongly tied to the surrounding temperature. The combination of declining tree vitality, an increasing frequency and magnitude of natural disturbances, and improved environmental conditions for insects has led to a significant intensification of bark beetle infestations across Europe (Biedermann et al., 2019).

This recent increase of infestations in central Europe has led to heightened interest in the remote sensing-based detection for forest management. Spruce trees *(Picea abies)*, the most prevalent tree species in central Europe, are especially vulnerable to changes in their environment, due to their shallow root system (Hlásny et al., 2021). With increasing availability of high-resolution spatial and temporal data, remote sensing has established itself as an essential tool for monitoring forest health and managing disturbances (Fassnacht et al., 2024). While remote sensing approaches in this field utilise a wide range of platforms and sensors, in-situ investigations are still the standard for detecting bark beetle infestations. However, these traditional methods are often constrained by difficult terrain, limited resources, and labour-intensive workflows, which can hinder their scalability and timely implementation (Luo et al., 2023).

Field surveys are currently the only reliable way to detect early signs of bark beetle infestations by locating boring dust or using pheromone traps (Marvasti-Zadeh et al., 2024). Therefore, the timing is the most important factor, as infested trees have to be located immediately after the successful colonisations, before the emergence of the brood. The development cycle of bark beetles typically takes around 6-10 weeks depending on weather conditions. During this timeframe, the infested tree undergoes the green-attack phase, defined as pre-visual before symptoms become visible to the human eye. Current remote sensing research focusses on this phase as an accurate identification of infested trees could greatly improve forest management strategies, as it enables timely interventions. However, detecting early bark beetle activity still remains challenging due to the structural/biochemical changes in trees being very subtle and as of yet not accurately detectable by optical remote sensing methods. Physiological signals can be detected prior to structual changes, however, they are still difficult to quantify with remote sensing methods (Kautz et al., 2024). Conversely, remote sensing approaches have proven effective for the retrospective analysis and quantification of infestation events. While these methods cannot directly aid sanitation efforts during active infesta-

This contribution has been peer-reviewed. The double-blind peer-review was conducted on the basis of the full paper.
https://doi.org/10.5194/isprs-annals-XI-3-2026-805-2026

tion phases, they are valuable for mapping and understanding outbreak patterns, providing insights into the spatial and temporal dynamics of bark beetle infestations (Fernandez-Carrillo et al., 2020).

The majority of studies in this research field rely on the use optical remote sensing data obtained from airborne systems or satellite platforms, such as Sentinel-2 and Landsat (Marvasti-Zadeh et al., 2024). In contrast, radar data has received less attention. The backscattered radar signal of VH and VV polarisations is particularly sensitive to vegetation water content and structural properties, respectively (Hollaus and Vreugdenhil, 2019). Both Sentinel-1 and Sentinel-2 have similar geometric as well as spatial resolution. However, radar's active sensing capabilities allow it to circumvent limitations of optical (passive) sensors, resulting from cloud cover or smoke. The addition of Sentinel-1 data increases the number of usable scences within a defined time period as it doesn't depend on weather conditions.

Therefore, the objective of this study is to evaluate the potential of Sentinel-1 radar data to detect bark beetle infestations. The achieved results are compared with the results achieved by a Sentinel-2-based approach. With an additional focus on the influence of topographical features on classification results.

2. Data and Study Area

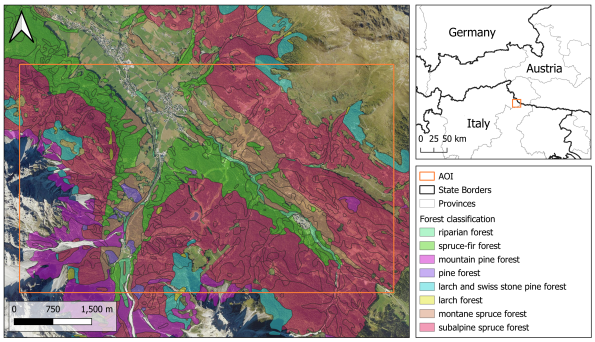

Figure 1. Overview of the study area in the Northern Italian Alps with forest classification.

The study area is located in the Northern Italian Alps, within the Autonomous Province of Bolzano/Bozen around the municipality of Sexten/Sesto. It covers approximately 32 km², about half of which is forested (Figure 1). The region is characterized by alpine terrain with typical topographical features, including steep slopes in all cardinal directions and valleys. The elevation ranges from 1,100 m a.s.l. at the valley bottom to nearly 3,000 m a.s.l. at the peaks of the Dolomites. At lower elevations, patches of deciduous forests are present on a local scale. However, the majority of forested area is dominated by dense coniferous forest, primarily spruce, with smaller, localized occurrences of Scots pine *(Pinus sylvestris)*, Swiss stone pine *(Pinus cembra)* and larch *(Larix decidua)* (Autonomous Province of Bolzano/Bozen, 2025).

This study utilised two Sentinel datasets covering the years 2020 to 2023. The Sentinel-1 dataset consisted of Ground Range Detected (GRD) data with VV and VH polarisations from both ascending and descending orbits, with a spatial resolution of 10m. The Sentinel-2 dataset spanned the same time period and consisted of the spectral bands used to compute the vegetation indices for the classification (Table 1). To ensure data quality, a cloud cover filter with a maximum threshold of 80% was applied to the Sentinel-2 dataset.

A forest mask was applied to limit the analysis on forested areas. As the study operated on a local scale the forest classification map of the Autonomous Province of Bolzano/Bozen is used (Autonomous Province of Bolzano/Bozen, 2025). The study area was limited to areas with spruce as the predominant tree species.

The reference dataset was provided by the Department of Forest Planning of the Autonomous Province of Bolzano/Bozen and was used to validate the results of the classification model. This dataset consisted of vector polygons labelling forested areas infested by bark beetles. While the dataset spans the period from 2017 - 2023, the number of polygons and the level of detail are limited for the years prior to 2021. As a result, the validation of classification results was restricted to the time period from 2021 to 2023. The dataset, containing data up to 2022, is available for download via the Geobrowser (Autonomous Province of Bolzano/Bozen, 2025).

3. Methods

The main workflow applied in this study is shown in figure 2 and is used for both Sentinel-1 and Sentinel-2 classifications. The pre-processing steps for each dataset are tailored to their respective characteristics. All Sentinel-1 scenes were pre-processed with the Sentinel-1 Toolbox (ESA, 2024b). The pre-processing workflow includes the removal of thermal noise, radiometric calibration and a terrain correction based on the SRTM 30m DEM. Sentinel-2 data was downloaded at the L1A (top of atmosphere) processing level and pre-processed using the Sen2Cor processor (ESA, 2024a). This step corrected for atmospheric, terrain and cirrus-related effects. The s2cloudless algorithm (Zupanc, 2017) was applied for cloud and shadow detection. After pre-processing, all spectral bands used in the analysis were resampled to a spatial resolution of 10m. A selection of vegetation indices was calculated based on findings of recent literature (see Table 1). These indices were chosen to represent different parts of the electromagnetic spectrum that are particularly sensitive towards vegetation changes. As bark bettle infestations alter the biochemical properties of needles, changes in tree vitality are detectable by deviations in needle relfectance. The green and red-edge regions are known to be sensitive to dehydration and insect attacks. The SWIR and NIR regions are responsive to changes in water content and nitrogen content (Abdullah et al., 2019).

Index	Formula	Reference
NDVI	$\frac{\text{NIR}-\text{RED}}{\text{NIR}+\text{RED}}$	(Bozzini et al., 2024)
GDVI	$\frac{\text{NIR}-\text{GREEN}}{\text{NIR}+\text{GREEN}}$	(Bozzini et al., 2024)
NDREI	$\frac{\text{NIR}-\text{RED-Edge1}}{\text{NIR}+\text{RED-Edge1}}$	(Abdullah et al., 2019)
NGRDI	$\frac{\text{GREEN}-\text{RED}}{\text{GREEN}+\text{RED}}$	(Abdullah et al., 2019)
SR_SWIR	$\frac{\text{NIR}}{\text{SWIR}}$	(Abdullah et al., 2019)
GLI	$\frac{\text{2*GREEN-RED-BLUE}}{\text{2*GREEN+RED*BLUE}}$	(Eng et al., 2019)

Table 1. Vegetation indices calculated for the Random Forest classification.

Yearly composties were created from both datasets. To minimize noise and uncertainty caused by snow, the analysis was restricted to the growing season (May - September). The temporal

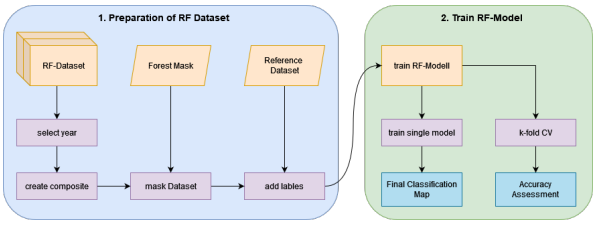

Figure 2. Applied workflow for the RF classification and data preparation.

limitation helped reduce artifacts in individual scenes, resulting in more robust classification results (Kollert et al., 2021). For all vegetation indices and both radar polarisations, statistical metrics - maximum, minimum, mean and standard deviation – were computed. Additionally, for each index and polarisations the difference between the annual mean and maximum values was calculated for each pixel. These derived metrics were subsequently used as input features for the classification model, resulting in 30 features per year.

For each year from 2021 to 2023, 150 pixels per class (healthy and infested) were labelled to be used as input features for the classification, resulting in a total of 300 labelled pixels per year and 900 pixels across the study period. A stratified random sampling approach was employed to select pixels from the reference dataset. Each labelled pixel included the corresponding vegetation indices and radar polarisations used for the classification.

In recent years, machine and deep learning approaches have become increasingly common in studies focussing on bark beetle infestations (Marvasti-Zadeh et al., 2024). In this study, a Random Forest (RF) classification model was implemented to differentiate between healthy and infested forest areas. The RF algorithm is widely used in remote sensing applications due to its flexibility, robustness and ease of implementation. It operates by constructing multiple decision trees, staring from a root node, growing banches, and determining the final classification through a majority voting process across the ensemble of trees (Breiman, 2001). The growth of each decision tree is controlled by a set of hyperparameters (Tab. 2).

Parameter	Value
N_ESTIMATORS	500
MAX_DEPTH	10
MIN_SAMPLES_SPLIT	2
MIN_SAMPLES_LEAF	4
MAX_FEATURE	sqrt
RANDOM_STATE	42
BOOTSTRAP	True

Table 2. Parameter settings.

The hyperparameters for the RF model were initially optimized using a nested k-fold cross validation (CV) approach. Although different hyperparameters were computed for each year and dataset, a single set of hyperparameters was defined to ensure consistency across all model runs. This standardization resulted in negligible changes in overall accuracy across all combinations. To determine the contribution of individual features to the final classification, the RF classification calculates feature importances (FI), which quantify the contribution of individual features to the final classification. It allows for the further refinement of the model and to improve performance and efficiency. The RF model was applied to both Sentinel-1 and Sentinel-2 datasets for all years and was implemented using a repeated stratified k-fold CV approach. Cross-validation was employed to train and test the model without requiring an additional validation dataset. The dataset was split into ten folds, with nine folds used for training and the remaining fold used for validation. This process was repeated ten times with different splits, resulting in 100 classifications per year and dataset. The stratification ensured that the class distribution was preserved across all folds and repetitions, providing a robust evaluation of the model’s performance.

The RF classification required the definition of input variables, referred to as features, which the model used to perform classifications. For the Sentinel-1 dataset, the features included both VV and VH polarisations with statistical metrics: maximum, minimum, mean and standard deviation. Additionally, the differences between maximum and mean values to the previous year were calculated and used as input features. This resulted in a total of 18 features per classification. For the Sentinel-2 dataset, which incorporated a larger number of VIs, the same statistical metrics were calculated, resulting in 36 features per classification. These statistical metrics were chosen to capture different processes occurring in the study area and reflect the impacts of bark beetle infestations.

When using Sentinel-2 data, the minimum and maximum values of the VIs were used to represent vegetation vitality and visible changes associated with bark beetle disturbances. The mean and standard deviation were included to capture gradual changes in vegetation over time. As trees undergo the decaying process, which includes distinct phases related to changes in the spectral reflectance, infested stands were expected to exhibit higher standard deviation values and lower mean values compared to healthy stands.

The dual-polarized Sentinel-1 radar data (VV and VH) were sensitive to different scattering mechanisms in forested areas. VV polarisation was sensitive to surface scattering, which is influenced by the structure and orientation of tree trunks and branches. This makes it useful for identifying later-stage infestations, with damaged forest canopies and an increased exposure of forest floor resulting in a change in backscatter values. Additionally, VV backscatter exhibited high sensitivity towards soil moisture, which increased in areas where bark beetle infestations caused tree mortality, leading to greater exposure of the soil surface. Additionally, transpiration as well as interception loss is reduced in deed trees (Hollaus and Vreugdenhil, 2019, Edburg et al., 2012).

The VH polarisation, on the other hand, is sensitive to volume scattering, which occurs when the radar signal interacts with the inner parts of vegetation, such as needles and smaller branches. In bark beetle-infested canopies, the VH signal is expected to decrease as vegetation density and structural complexity are reduced (Hollaus and Vreugdenhil, 2019). The differences in mean and maximum values compared to previous years enabled the detection of temporal dynamics associated with bark beetle disturbances. Significant deviations could indicate major changes in the forest canopy, caused by severe infestations or subsequent salvage logging activities. These temporal changes were observable in both Sentinel-1 and Sentinel-2 datasets (cf. Sect. 4).

This contribution has been peer-reviewed. The double-blind peer-review was conducted on the basis of the full paper.
https://doi.org/10.5194/isprs-annals-XI-3-2026-805-2026 | © Author(s) 2026. CC BY 4.0 License.

The accuracy assessment was performed using a binary confusion matrix. To evaluate the classification results, overall accuracy (OA) values were calculated for all years and both datasets. The OA metric compares the number of correctly predicted samples for both classes to the total number of predictions, making it the most widely used metric to evaluate the performance of a classification. To assess the stability of the classification results, the range of OA values obtained during the repeated cross-validation process was visualized using boxplot diagrams. This allowed assessing the variability of the model’s performance across different folds and repetitions. The achieved accuracies for all combinations, along with the corresponding feature importance values, are discussed in the following section. Additionally, to provide a visual representation of the classification results, a single model was trained using the entire reference dataset. This visualization was generated for both Sentinel-1 and Sentinel-2 datasets, enabling a direct comparison of the results obtained from the two data sources.

4. Results

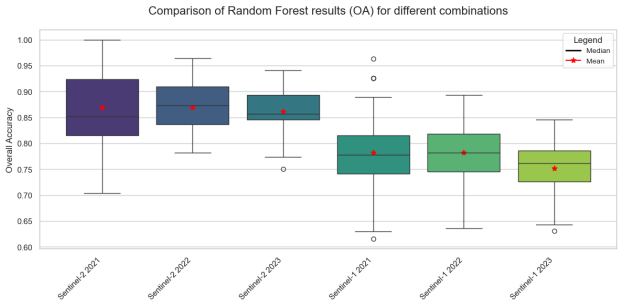

Figure 3. Comparison of overall accuracies values of RF classifications based on year and dataset.

Figure 3 illustrates the distribution of classification results for different years and datasets. The classifications based on yearly Sentinel-1 composites achieved an average overall accuracy of 0.77 across all years, with 2023 reporting the lowest OA. The range of accuracy values is most pronounced in 2021 with some statistical outliers observed in both directions. In contrast, no statistical outliers were detected for 2022, with the range of values being comparable to the previous year. In 2023, the range of accuracy values had decreased, indicating improved consistency in the model’s performances.

For classifications based on vegetation indices derived from Sentinel-2 data, the average OA reached 0.85. The range of overall accuracy values was most pronounced in 2021 with subsequent years showing more concentrated accuracy distributions. Across all three years, the average OA only varied slightly, indicating a strong consistency of the model throughout the study period. On average, the OAs achieved using Sentinel-1 data were 10% lower than with Sentinel-2 data.

In the first year (2021), the mean yearly values of both VV and VH polarisations, as well as the mean difference of VV polarisation between 2020 and 2021 were attributed the highest feature importance (Fig. 4). These three features also maintained high importance in 2022, with the mean difference of the VH polarisation identified as an additional key feature for the classification model. In 2023, the feature importance values were more evenly distributed, with the mean differences of VV and VH polarisations compared to the previous year being the most significant.

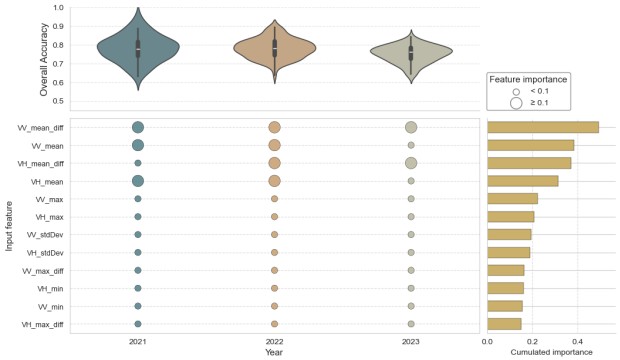

Figure 4. RF feature importance for the classification setup using Sentinel-1 data with yearly composites. Feature importance values are averaged across all folds. Violin plots on top depict the distribution of OA values for each year. The horizontal bars show the cumulative importance of each feature used.

The yearly mean values of VV and VH polarisation, along with the mean differences between years, showed the highest cumulated feature imporance values (Fig. 4). The maximum yearly values of both polarisations also contributed significantly, although to a lesser extent. In contrast, the maximum differences between years showed below-average performance. The minimum values of both polarisations had minimal contribution to the final classification, while the standard deviation of both polarisations demonstrated moderate importance.

Figure 5 shows the mapped results of the RF classifications for the year 2023, with the left map displaying the results derived from Sentinel-1 data and the right map from Sentinel-2 data. The results reveal that bark beetle infestations were concentrated in two primary clusters within the study area. The eastern infestation hotspot on the south facing slope was more pronounced in the Sentinel-1-based classification, with additional areas further southeast also identified as infested. In contrast, the scythe-shaped infestation cluster on the north eastern slope was less prominent in the Sentinel-1 classification, with only small, distinct forest stands being classified as infested. In the central part of the study area, the Sentinel-1-based classification identified smaller, scattered infestation areas that were not detected by the Sentinel-2-based classification.

In Figure 6 and 7 the distribution of slope and aspect values of the input features are shown, respectively. The aspect values were grouped into cardinal and intercardinal directions resulting in eight bins. To allow for the comparison of results, the slope values were also binned accordingly. The distribution of aspect values (Figure 6) revealed a clear overrepresentation of pixel in south and southwest as well as north and northwest-facing directions. The relative frequency of misclassified pixels with Sentinel-1 data depicted a similar pattern with the highest frequencies being recorded in the same directions. With the exception of west-facing slopes, which showed an overrepresentation of misclassified pixels. For the classification with the Sentinel-2 dataset, a different pattern was observed. Misclassification rates deviated from the total number of pixels, with the highest rates being recorded for the southeast direction.

On the other hand, the distribution if slope values for all accumulated pixels (Fig 7) revealed, that the majority of classified pixels had a slope value between 15°and 30°, with only a limited number of pixels at steeper or flatter inclinations. For Sentinel-1 data, the relative frequency of misclassified pixels

https://doi.org/10.5194/isprs-annals-XI-3-2026-805-2026

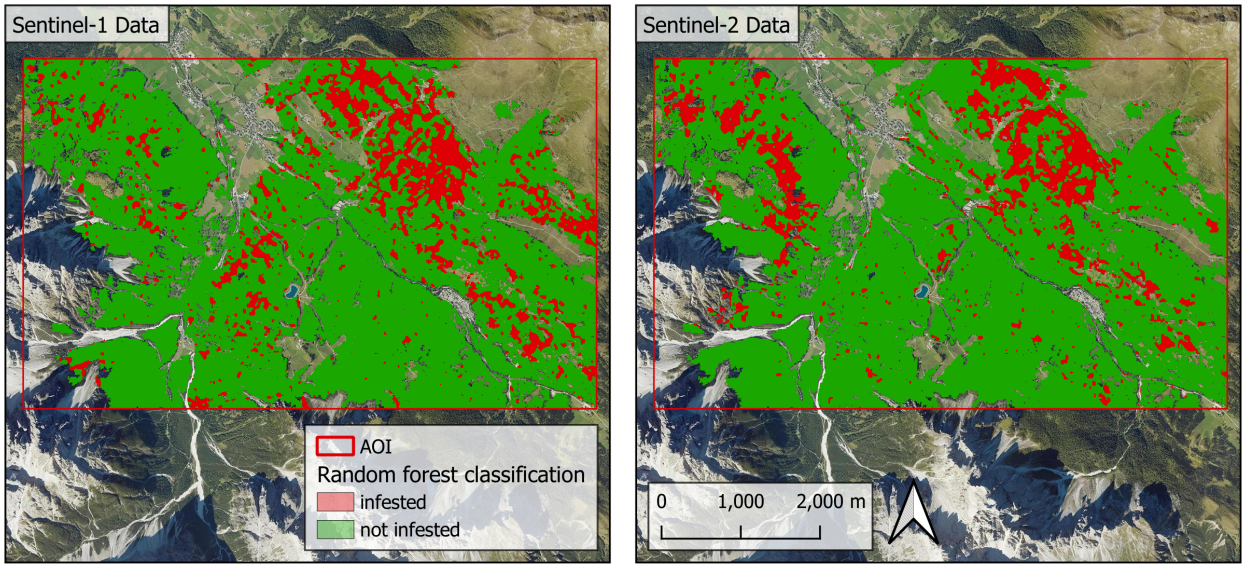

Figure 5. Map of the RF results with Sentinel-1 and Sentinel-2 data for 2023.

depicted a clear clustering of misclassifications around higher slope values, with ratios exceeding 30% between 25°and 40°. Less inclined pixel showed a lower relative frequency of misclassified features. More inclined pixels as well yielded a lower relative frequency, albeit, the number of total pixels for this inclination was already very low. For Sentinel-2 data, Pixels with slope values >40°demonstrated the highest misclassification rates, exceeding 30%. Between 25°and 40°, the relative frequency of misclassified pixels was higher than for less inclined slopes, however, not as pronounced as for Sentinel-1 data.

5. Discussion

The results of the RF classification underscore the potential of radar data for detecting bark beetle infestations. While the RF model trained on Sentinel-1 data was consistently outperformed by the model trained on Sentinel-2 data, the average difference in overall accuracy between the two models was less than 0.1. The RF classifications for both datasets demonstrated strong consistency across all years, with average OA values varying only slightly (Fig. 3).

The employed approach utilised yearly growing season composites to detect bark beetle disturbances. The use of composites enhanced the robustness of classification results by reducing noise and artifacts in the dataset. However, this method has limited potential for early detection of bark beetle infestations. The primary focus of the study was to analyse the capability of Sentinel-1 data to detect bark beetle infestations at later stages. Late-stage infestation detection often corresponds to significant damage in affected forest stands, where changes in spectral properties and radar backscatter become more pronounced due to alterations in surface scattering within the canopy. Radar backscatter is strongly influenced by surface-specific scattering mechanisms, which are determined by geometric and electromagnetic properties, with the electric permittivity being the most critical. Since vegetation primarily consists of water, the dielectric constant, which quantifies to the amount of backscattered energy, increases with higher biomass and moisture levels (Hollaus and Vreugdenhil, 2019). Bark beetle infestations induce water stress in affected trees, leading to a decline in moisture content. This reduction could potentially be detected through time series analysis of Sentinel-1 data, allowing for early detection approaches. Although it has to be noted that the deviations of the results achieved of both datasets were not too significant, indicating the high potential of Sentinel-1 data even when combined with a workflow designed for optical data. The insights gained suggest that phenological composites are a valuable tool for dectecting bark beetle infestations.

The feature importance analysis revealed two features - the yearly mean values of VV and VH polarisations - most important for the RF classification. The mean provided a measurement of the overall forest condition during a year, offering insights into vegetation vitality. By combining all scenes of the vegetation period, it was possible to filter out variations as well as data noise,thereby improving model performance. Changes in tree vitality associated with later-stage bark beetle infestations — such as changes in needle colour and loss of needles — occur gradually in the weeks following initial infestation. These changes were reflected in the mean values of radar backscatter and vegetation indices, leading to a decrease in mean values.

The mean differences of VV and VH polarisations between consecutive years were also highly weighted by the classification. These features captured the trend of change in vegetation vitality by comparing mean values across two years. An infestation occurring in the second year would result in a deviation in mean polarisation values compared to the previous year, which was subsequently reflected in the RF classification results. The high importance of these calculated differences underscorese their potential application in early detection of bark beetle infestations, as they can highlight subtle changes in vegetation health before significant damage becomes visible.

In contrast, the maximum differences between consecutive years were not strongly weighted. The maximum value represents the highest backscatter value observed for each pixel within a given year. While maximum values in optical data are often interpreted as the peak of vegetation activity, for radar data, the

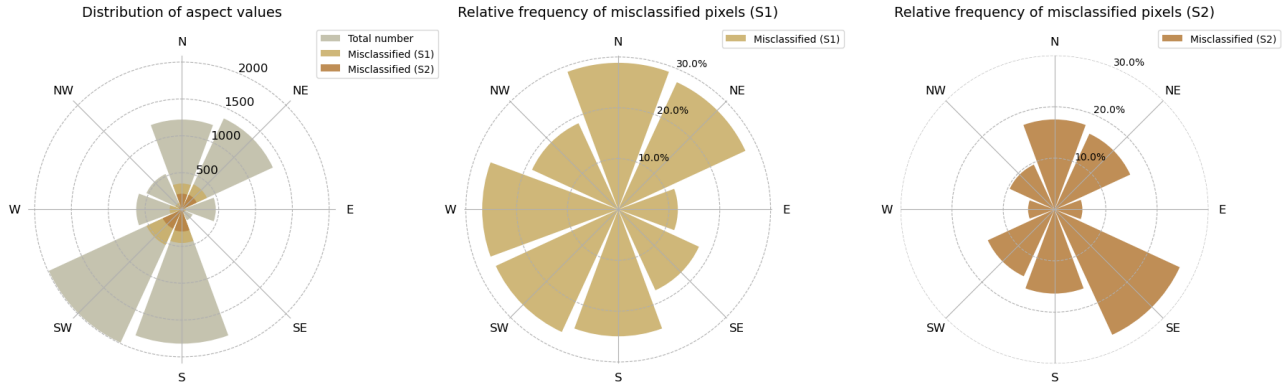

Figure 6. Distribution of aspect values of pixels used as features for the RF classification. The left plot shows the cumulated number of aspect values with the fraction of misclassified pixels for all classifcations with Sentinel-1 and Sentinel-2 data. The remaining two plots show the relative frequency of misclassifed pixels for Sentinel-1 and Sentinel-2, respectively.

maximum backscatter value reflects the structural and volumetric properties of the forest. The VV polarisation is primarily influenced by surface scattering, while the VH polarisation is sensitive to volume scattering from the forest canopy (Hollaus and Vreugdenhil, 2019).

Unlike vegetation indices, the maximum backscatter value did not strictly follow phenological trends and was siginifcantly affected by outliers. Additionally, these values can be influenced by environmental factors, such as rainfall or snow moisture, which temporarily increases backscatter. This variability reduced the reliability of maximum values as indicators of bark beetle disturbances, explaining their comparatively lower feature importance in the RF classification. Similarly, the minimum values of both polarisations also exhibited low feature importance as they were more susceptible to noise and outliers (Edburg et al., 2012).

The standard deviations of VV and VH polarisations provided valuable information about the temporal variability of forest conditions. For the VV polarisation, a high standard deviation reflected significant changes in forest structure, leading to variations in surface scattering and increased variability in VV backscatter. Similarly, a high standard deviation of the VH polarisation indicated changes in volume scattering, which are typically associated with alterations in canopy density. High standard deviation values can signify disturbances of forest stands. Despite this, the feature importance of both standard deviations were not heavily weighted by the classification. This suggests that while standard deviation values could detect differences between infested and healthy forest stands, the differentiation was more difficult compared to other features, such as mean values or mean yearly differences (Hollaus and Vreugdenhil, 2019).

The results shown in Figure 5 visualize the mapped results of both RF classifications. The classification based on Sentinel-2 data revealed two primary infestation clusters, with some additional, more localized infestation areas detected across the study area. However, these smaller areas did not exhibit a clear spatial pattern, suggesting they represented isolated or less severe disturbance events. The large cluster in the north western part of the study area was only sparsely detected by the Sentinel-1-based model, with some local clusters being classified as infested. On the other hand, the second major cluster on the opposite side of the study area was overrepresented by the Sentinel-1 classification in comparison to Sentinel-2. These discrepancies may be attributed to the acquisition characteristics of the Sentinel-1 satellites and their interaction with complex topography. Unlike Sentinel-2, which collects data vertically from directly above, Sentinel-1 satellites acquire data at an incidence angle, capturing information sideways, which is essential for constructing two-dimensional images using range and azimuth — a key process in synthetic aperture radar imaging (ESA, 2024b).

To account for topography, the influence of slope and aspect was analysed for both sensor types. The distribution of aspect values across the study area (Fig. 6) shows a clear clustering of aspect values in the north/northeast as well as south/southwest direction. These directions also yielded the highest relative frequency of misclassified pixels for Sentinel-1-based classifications. Therefore, a linear correlation between the total number of pixels per direction and the relative frequency of misclassified pixels could be suspected, with an exception in the west direction. The total number of pixels in this direction was lower in comparison, however, the rate of misclassified pixels also exceeded 20%. This contrasted the remaining three directions (E, SE and NW), which showed significantly lower misclassification rates. Both distributions, however, did not show a clear pattern towards this topographic feature, with the relative frequency of misclassified pixels increasing linear with the total number of pixels in each direction. On the contrary, for the classification based on Sentinel-2 data, the highest misclassification rates were recorded in southeast direction, albeit, with the lowest number of pixels in this direction. The other directions exhibited a similar pattern to the Sentinel-1-based results. Although, with lower relative frequencies, as the achieved overall accuracy was higher.

On the other hand, the distribution of slope values exhibited a more pronounced trend (Fig. 7). The distribution of slope values revealed that the majority of pixels has a slope value between 15°and 30°, as the class 25°- 30°was the most prevalent. More and less steep inclinations recorded lower absolute numbers of misclassified pixels. Contrasting results were observed for the relative frequency of misclassified pixels. For the Sentinel-1-based classification, a clear increase of misclassifications at stepper slopes could be observed, resulting in misclassification rates >30% for slope classes between 25°and 40°. Only a limited number of pixels had a higher slope value (>40°), resulting in a lower relative frequency. Less inclined pixels exhibited a lower misclassification rate, with a higher total number of pixels. On the contrast, the misclassifica-

This contribution has been peer-reviewed. The double-blind peer-review was conducted on the basis of the full paper.
https://doi.org/10.5194/isprs-annals-XI-3-2026-805-2026 | © Author(s) 2026. CC BY 4.0 License.

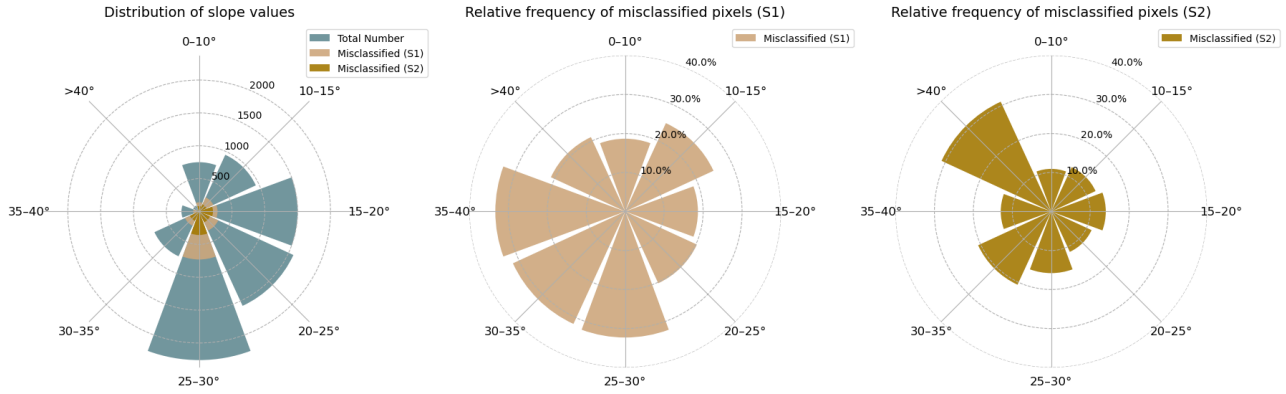

Figure 7. Distribution of slope values of pixels used as features for the RF classification. The left plot shows the cumulated number of slope values with the fraction of misclassified pixels for classifcations with Sentinel-1 and Sentinel-2 data. The remaining plots show the relative frequency of misclassifed pixel cumulated over all years for both datasets. All slope values are binned to allow for better comparability.

tion rates for the Sentinel-2-based classification were most pronounced for slopes >40°, with of over 30%. The other misclassification rates corresponded to the results achieved with Sentinel-1 data, showing relatively higher rates for steeper inclined pixel. Both achieved results showed that for slope values, the relative frequency of misclassified pixels didn't directly correlate to the number of pixels per class. Additionally, this observed trend was less pronounced than for the classification based on Sentinel-1 data.

To summarize, the evaluation of the impact of topography on the classification results didn't provide a clear picture. The topographical features aspect and slope were selected to determine the influence of mountainous terrain on the backscatter values of radar data and consequently on classification accuracies. Both features revealed diverging influences on both classifications. The aspect values of the Sentinel-1 classification showed a linear correlation between the total number of pixels per direction and the relative frequency of misclassified pixels, albeit, with some smaller outliers. For the Sentinel-2 classifications, the south west direction was detected as an outlier, most likely a result of limited data availability. The remaining directions showed similar misclassification ratios as the Sentinel-1-based classification. Therefore, no clear influence pattern of this topographic feature on the classification results could be observed.

The slope values, on the other hand, did exhibit a clear deviation from this linear pattern and showed a deviating distribution. The relative frequency of misclassified pixels increased with steeper inclination values and didn't correspond directly to the number total number of pixels per bin. Revealing a trend towards higher misclassification rates with increasing inclination. This trend was observable for both classifications, however, it was more pronounced for the classification with Sentinel-1 data. The classification based on Sentinel-2 data showed a significant outlier (>40°) with misclassification rates >30%.

However, it cannot be ruled out that secondary factors influenced the distribution of both topographic features. To further evaluate the influence of topography on classification results, more topographical features need to be integrated. Furthermore, the interpretability of results could be improved by incorporating a balanced distribution of values for each direction and aspect class. However, the comparison still revealed, that the topographic features examined, did have a different influence on the classification results with distinct patterns being detected.

Additional studies are required to evaluate the possibilities of radar data, for the early-detection of bark beetle infestations. Bark beetle infestations induce water stress in infested trees, reducing water content in the needles due to stomata closing to prevent further water loss. Photosynthesis and transpiration are therefore limited, resulting in increased needle temperature. As the water content relates directly to the dielectric constant which controls backscatter, a reduction in water content leads to relatively lower backscatter in comparison to healthy trees (Hollaus and Vreugdenhil, 2019). This difference in backscatter could be detected with radar sensors, depending on the magnitude of difference and sensor used.

6. Conclusion

The presented study employed phenological composites of Sentinel-1 data to evaluate its potential to detect bark beetle disturbances and compareed the results to those achieved with Sentinel-2 data. Composites of VV and VH polarisations were used to identity changes in surface or volume backscattering, respectively. The RF classification based on Sentinel-1 composites achieved an average OA of 0.75 for detecting changes associated with later-stage bark beetle infestations, while the same classification setup using vegetation indices derived from Sentinel-2 data achieved a higher average OA of 0.87.

The results of this study indicate that standardized workflows, designed for optical, multispectral data are not fully suited for direct application to radar data, albeit, still achieving respectable results. Developing workflows specifically adapted to the unique characteristics of radar data could further improve classification accuracies and infestation detection rates. Implementing a robust pre-processing pipeline is essential to address geometric and topographic distortions, particularly in complex mountainous terrain where topography significantly influences radar backscatter. Optical sensors also have their own limitations, such as sensitivity to weather conditions. By properly accounting for the limitations of both optical and radar data, their integration can enhance workflows and improve the accuracy of classification results.

Topography also influenced classification accuracies. The topographic features slope and aspect directly contributed to the frequency of misclassifications. Albeit, to a varying degree with slope values showing a strong correlation between higher frequencies of misclassified pixels with increasing steepness. The

implementation of additional topographic features is needed to evaluate the influence of topography on classification results. Further research is needed to explore the potential of radar data, particularly Sentinel-1, for (early) detection of bark beetle infestations. By addressing current limitations and refining workflows, the integration of radar and optical data could lead to more accurate and comprehensive forest health monitoring systems.

7. Acknowledgements

This study was conducted within the framework of the research project ”BeatTheBeetle - Early detection of the spruce bark beetle in Austria using remote sensing”, funded by the Austrian Research Promotion Agency (FFG), Austria Space Program (ASAP).
The authors would also like to thank the Department of Forest Planning of the Autonomous Province of Bozen - South Tyrol for providing the reference dataset of bark beetle infestations.
During the preparation of this work the authors used Academic AI in order to improve the readability and grammar of the manuscript. The authors made subsequent adjustments and take full responsibility for the content of the publication.

References

Abdullah, H., Skidmore, A. K., Darvishzadeh, R., Heurich, M., 2019. Sentinel-2 accurately maps green-attack stage of European spruce bark beetle (*Ips typographus* , L.) compared with Landsat-8. *Remote Sens Ecol Conserv*, 5(1), 87–106.

Autonomous Province of Bolzano/Bozen, 2025. Geobrowser. https://natur-raum.provinz.bz.it/de/geobrowser-maps. Accessed: 2025-10-01.

Biedermann, P. H., Müller, J., Grégoire, J.-C., Gruppe, A., Hagge, J., Hammerbacher, A., Hofstetter, R. W., Kandasamy, D., Kolarik, M., Kostovcik, M., Krokene, P., Sallé, A., Six, D. L., Turrini, T., Vanderpool, D., Wingfield, M. J., Bässler, C., 2019. Bark Beetle Population Dynamics in the Anthropocene: Challenges and Solutions. *Trends in Ecology & Evolution*, 34(10), 914–924.

Bozzini, A., Brugnaro, S., Morgante, G., Santoiemma, G., Deganutti, L., Finozzi, V., Battisti, A., Faccoli, M., 2024. Drone-based early detection of bark beetle infested spruce trees differs in endemic and epidemic populations. *Front. For. Glob. Change*, 7, 1385687.

Breiman, L., 2001. Random Forests. *Machine Learning*, 45(1), 5–32.

Edburg, S. L., Hicke, J. A., Brooks, P. D., Pendall, E. G., Ewers, B. E., Norton, U., Gochis, D., Gutmann, E. D., Meddens, A. J., 2012. Cascading impacts of bark beetle-caused tree mortality on coupled biogeophysical and biogeochemical processes. *Frontiers in Ecol & Environ*, 10(8), 416–424. https://esajournals.onlinelibrary.wiley.com/doi/10.1890/110173.

Eng, L. S., Ismail, R., Hashim, W., Baharum, A., 2019. The Use of VARI, GLI, and VIgreen Formulas in Detecting Vegetation In aerial Images. *IJTech*, 10(7), 1385.

ESA, 2024a. Sen2cor v2.12: A processor for sentinel-2 level-2a product generation. https://step.esa.int/main/snap-supported-plugins/sen2cor/.

ESA, 2024b. Sentinel-1 products specification. https://sentiwiki.copernicus.eu/web/s1-products. Accessed: 2024-10-10.

Fassnacht, F. E., White, J. C., Wulder, M. A., Næsset, E., 2024. Remote sensing in forestry: current challenges, considerations and directions. 97(1), 11–37.

Fernandez-Carrillo, A., Patočka, Z., Dobrovolný, L., Franco-Nieto, A., Revilla-Romero, B., 2020. Monitoring Bark Beetle Forest Damage in Central Europe. A Remote Sensing Approach Validated with Field Data. *Remote Sensing*, 12(21), 3634.

Hlásny, T., König, L., Krokene, P., Lindner, M., Montagné-Huck, C., Müller, J., Qin, H., Raffa, K. F., Schelhaas, M.-J., Svoboda, M., Viiri, H., Seidl, R., 2021. Bark Beetle Outbreaks in Europe: State of Knowledge and Ways Forward for Management. *Curr Forestry Rep*, 7(3), 138–165.

Hollaus, M., Vreugdenhil, M., 2019. Radar Satellite Imagery for Detecting Bark Beetle Outbreaks in Forests. *Curr Forestry Rep*, 5(4), 240–250.

Huang, J., Kautz, M., Trowbridge, A. M., Hammerbacher, A., Raffa, K. F., Adams, H. D., Goodsman, D. W., Xu, C., Meddens, A. J. H., Kandasamy, D., Gershenzon, J., Seidl, R., Hartmann, H., 2020. Tree defence and bark beetles in a drying world: carbon partitioning, functioning and modelling. *New Phytologist*, 225(1), 26–36.

Kautz, M., Feurer, J., Adler, P., 2024. Early detection of bark beetle (Ips typographus) infestations by remote sensing – A critical review of recent research. *Forest Ecology and Management*, 556, 121595.

Kollert, A., Bremer, M., Löw, M., Rutzinger, M., 2021. Exploring the potential of land surface phenology and seasonal cloud free composites of one year of Sentinel-2 imagery for tree species mapping in a mountainous region. *International Journal of Applied Earth Observation and Geoinformation*, 94, 102208.

Luo, Y., Huang, H., Roques, A., 2023. Early Monitoring of Forest Wood-Boring Pests with Remote Sensing. *Annu. Rev. Entomol.*, 68(1), 277–298.

Marvasti-Zadeh, S. M., Goodsman, D., Ray, N., Erbilgin, N., 2024. Early Detection of Bark Beetle Attack Using Remote Sensing and Machine Learning: A Review. *ACM Comput. Surv.*, 56(4), 1–40.

Seidl, R., Schelhaas, M.-J., Lexer, M. J., 2011. Unraveling the drivers of intensifying forest disturbance regimes in Europe. *Global Change Biology*, 17(9), 2842-2852.

Seidl, R., Thom, D., Kautz, M., Martin-Benito, D., Peltoniemi, M., Vacchiano, G., Wild, J., Ascoli, D., Petr, M., Honkaniemi, J., Lexer, M. J., Trotsiuk, V., Mairota, P., Svoboda, M., Fabrika, M., Nagel, T. A., Reyer, C. P. O., 2017. Forest disturbances under climate change. *Nature Clim Change*, 7(6), 395–402.

Turner, M. G., 2010. Disturbance and landscape dynamics in a changing world. *Ecology*, 91(10), 2833–2849.

Zupanc, A., 2017. Improving cloud detection with machine learning. https://medium.com/sentinel-hub/improving-cloud-detection-with-machine-learning-c09dc5d7cf13. Accessed: 2025-10-01.